231 (2023) 212312

Contents lists available at ScienceDirect

Geoenergy Science and Engineering

journal homepage: www.sciencedirect.com/journal/geoenergy-science-and-engineering

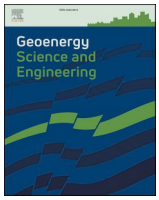

"Characteristic features of shale barrier materials"

Erling Fjær [*], Jørn F. Stenebråten, Sigurd Bakheim [1], Idar Larsen

Applied Geoscience, SINTEF Industry, S.P. Andersens veg 15b, 7031, Trondheim Norway

A B S T R A C T

Deep wells in soft formations are completed with a steel tube ("casing") that isolates the well from the surrounding rock. The annulus between the casing and the rock is usually left open in long sections of the well, thus creating a potential pathway for leakage which must somehow be sealed by a barrier. In many wells, it has been observed that shale formations creep in and close the annulus all by themselves, thus creating *shale barriers*. This may represent huge cost savings for the operator. However, this does not happen in all shale formations. It is therefore of great interest for the operator to identify at an early stage whether a given shale is a potential shale barrier material.

The objective of this study was to identify some characteristic features of shale barrier materials, that may allow for early identification and classification of shales in terms of their potential as shale barrier material. In this study, the performance of shale barriers created in laboratory tests have been compiled with several characteristic properties for a set of shale materials. As a first step in this process, a quantitative classification of the shales' willingness to form barriers was established, based on their resistance against annulus closure, and their resistance against forming a sealing barrier. The definitions of these parameters reflect that formation of shale barriers depends on several factors in addition to rock properties.

Porosity emerges as a key parameter from this study. This result is supported by theoretical considerations. High porosity implies low shear stiffness and strength which is a requirement for a shale barrier material. Low porosity on the other hand is often associated with over-consolidation and brittle behaviour which is unfavourable for the process of forming a sealing barrier by deformation of the rock. An interesting implication of this result is that several other parameters that are often available from well logs, such as density, and P- and S-wave velocities, may be used as indicators for shale barrier potential, since they are all closely related to porosity.

Contrary to expectations, the test results revealed only weak connection between shale barrier quality and mineralogy related parameters such as total clay content and quartz content. A possible explanation may be the limited selection of materials in our study, which contained only shales with clay content above 45% and quartz content below 30%. This result may indicate that clay content is less important if it is higher than a given threshold, and that quartz content is less important if it is lower than a given threshold.

1. Introduction

Wells providing the connection between hydrocarbon reservoirs and the surface infrastructure penetrate the cap rock that has prevented leakage from these reservoirs since their origin. Unless they are properly sealed, these wells represent potential pathways for leakage, also after they have been abandoned. Such wells are usually constructed with a steel tube ("casing") that constitutes an outer wall that protects the well from the formation outside. The casing is anchored to the formation by a cement plug, but long sections of the annulus between the casing and the rock around the hole are usually left open. An open annulus is a highly efficient pathway for flow of oil and gas, thus there is a need to seal off such open sections at critical locations within the cap rock, to prevent leakage along the well.

Ideally, we would like the annulus to be filled with a material that has the same sealing efficiency, the same chemical composition, and similar mechanical properties as the cap rock itself. Virtually infinite amounts of such a material are of course available right next to the well. Moreover, nature is also providing a considerable force – the in situ stress – that pushes this material towards the well. Numerous observations (Williams et al., 2009; Kristiansen et al., 2018, 2021; Noble et al., 2019) have shown that in some shale sections, the rock does indeed creep in and close the annulus, all by itself, forming a so called *shale barrier*. Shale barriers represent a huge cost saving potential for the operator, especially during plug and abandonment (P&A) operations, as it may eliminate the need for costly cementing operations (Vrålstad et al., 2019).

The formation of a shale barrier depends on a favorable combination of in situ conditions, borehole conditions, and rock properties. Borehole conditions are to some extent controllable, and it is intriguing that this may offer a potential for manipulation of the likelihood for the formation of a shale barrier. Rapid pressure drop in the annulus (Kristiansen

* Corresponding author.
E-mail address: erling.fjaer@sintef.no (E. Fjær).
[1] Current affiliation: STRATUM Reservoir, Trondheim, Norway.

https://doi.org/10.1016/j.geoen.2023.212312
Received 7 June 2023; Received in revised form 16 August 2023; Accepted 5 September 2023
Available online 9 September 2023

et al., 2018, 2021), heating of the borehole (Bauer et al., 2017; Xie et al., 2020), and annular fluid chemistry change (van Oort et al., 2020; Gawel et al., 2021) are all methods that affect the shale barrier formation process and are considered as potential methods to activate shales to form well barriers (Fjær and Larsen, 2018). It is not yet clear however to what extent these methods may actually change the overall likelihood for the formation of a shale barrier, or just accelerate a process that would happen naturally anyway as seems to be the case for annulus pressure drop (Kristiansen et al., 2021). It is therefore clearly of interest to be able to identify, as early as possible, whether a given shale is a good candidate as shale barrier material.

Earlier studies (Williams et al., 2009; Fjær et al., 2016; Kristiansen et al., 2018, 2021; Enayatpour et al., 2019; Holt et al., 2019, 2020; van Oort et al., 2022) have listed several features that appear to be characteristic for shale barrier materials:

Rock mechanical properties:

- Low shear stiffness, low Young's modulus
- Low cohesion, low unconfined compressive strength
- Low friction angle
- Ductile behavior

Mineralogy:

- High total clay content
- High smectite content
- Low matrix cementation
- Low content of quartz and carbonates
- High cationic exchange capacity

Petrophysical properties:

- Low permeability
- High porosity
- Low P-wave velocity

It has been the objective of this study to illustrate quantitatively how these characteristic features, and a few others, correlate with their willingness to form shale barriers.

2. Elementary considerations

The formation of a shale barrier requires that the force that pushes the rock towards the casing is higher than the strength of the stress arch that counteracts the movement of the rock. This force is given by the difference between the in situ stress and the annulus pressure, while the strength of the stress arch is given by the shear stiffness and shear strength of the rock.

One interesting result can be derived already from this recognition: Shales with low shear stiffness and strength are the best candidates as shale barriers since such shales cannot sustain large shear stresses. For the very same reason, the in situ stress carried by these shales cannot be largely anisotropic. In situ stress anisotropy may thus be an indicator for the shale's inferior quality as a shale barrier material.

Another interesting result that can be derived from the above recognition is related to the fact that the rock is pushed towards the casing by the compressive stress in the plane normal to the borehole axis. In a normal stress regime, where the vertical stress is larger than the horizontal stresses, we may therefore expect that the likelihood for shale barrier formation increases with well inclination.

Some other elementary relations can be established by making a few simplifying assumptions. First, we assume that the annulus pressure is equal to the in situ pore pressure, which is likely to happen eventually if there is hydraulic communication between the annulus fluid and the pore fluid. Further, we assume that the in situ stress is isotropic in the plane normal to the borehole axis, and that the rock deforms as an isotropic, linearly elastic material with shear stiffness G. The annulus will then be closed if the following requirement is fulfilled:

$$\sigma_h - p_{fo} > 2G\frac{\Delta R}{R} \tag{1.1}$$

where σ_h is the in situ stress, p_{fo} is the pore pressure, R is the borehole radius and ΔR is the gap between the casing and the borehole wall. As $\Delta R/R$ is typically 0.2–0.25 while σ_h - p_{fo} is of the order 10^1 MPa, we find that this requirement will be fulfilled only if $G << 0.1$ GPa. This is exceptionally low, requiring most likely that the deformation process involves a significant amount of plastic strain (Fjær et al., 2016).

For rocks that do not fulfill the requirement (1.1), the shear stress at the borehole wall may exceed the shear strength of the rock, if the in situ stress is sufficiently large. Assuming that the rock behaves like a linearly elastic material up until peak stress, we find that failure at the borehole wall may happen if

$$\sigma_h - p_{fo} > \frac{C_0}{2} \tag{1.2}$$

Failure at the borehole wall implies that parts of the rock may move into the annulus, but proper closure of the annulus will only happen if the post-peak deformation of the rock is predominantly ductile. Otherwise, the annulus may be partly filled with rock fragments that provides some relief for the stress arch but do not provide complete closure and proper sealing of the annulus.

We note that (1.1) is a sufficient requirement for annulus closure. On the other hand, if (1.1) does not occur, (1.2) is a necessary but not sufficient requirement for annulus closure. Although the question of closure or no closure of the annulus is a rock mechanical problem, there is apparently not a single rock mechanical parameter – or a simple combination of such parameters – that dictates whether the shale will form a sealing barrier or not.

3. Equipment and test procedures

A dedicated laboratory test, which we call a *shale barrier test,* has been designed to investigate whether a shale material is able to form a sealing barrier around a casing under given conditions. A description of the test and the equipment was given by Fjær et al. (2018).

The test is designed to simulate, as closely as possible, the geometry and stress conditions around a borehole. The shale sample is prepared as a hollow cylinder and exposed to an external stress that represents the in situ stress. The outer diameter is usually 4" (about 10 cm), to enable the use of field material that is available as seal peels. The ratio between the hole diameter and the outer diameter is set to 1:10, as a tradeoff between the need for a hole with sufficient size for instrumentation and the desire to minimize the effects of a finite sample size. The formation of a shale barrier implies that a region around the hole is largely deformed and most likely loses a part of its loadbearing capacity. If this region reaches the outer boundary of the sample, the sample is destabilized and the correspondence between the external stress and the in situ stress can no longer be trusted (Fjær et al., 2017).

The shale barrier tests are time consuming, lasting typically for a month or more. Along with limited access to test material, this makes repetition of uncomplete or non-ideal tests challenging or even impossible. In some cases, we have therefore been compelled to try to correct for shortcomings in the test rather than repeating it.

Fig. 1 illustrates the instrumented sample and the pressure configuration on the sample. The sample is placed between two steel end-pistons and a flexible sleeve extends over the sample between the end-pistons to act as a barrier between the sample and the fluid in the pressure vessel. A thin-walled aluminum tubing with an outer diameter of 8 mm is placed in the center hole. This tubing represents the casing, and it is instrumented internally with three strain gages which are calibrated with respect to uniform external pressure. The strain gages mounted in the casing measure the load on the casing continuously.

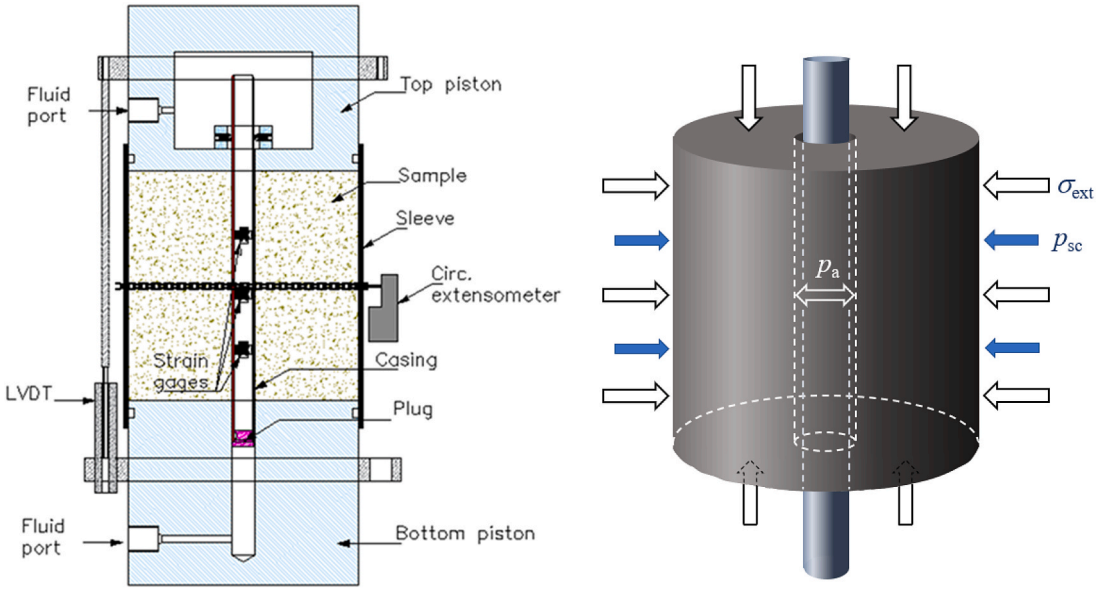

Fig. 1. Test cell configuration, sample, and pressures.

External strains of the sample are measured axially by LVDT's and radially with a circumferential extensometer.

The isotropic external stress (σ_{ext}) is identical to the pressure in the pressure vessel and acts axially and radially on the sample through the end-pistons and the sleeve. This stress represents the horizontal stress in a field situation with a vertical well.

The pore pressure on the external circumference (p_{sc} – called "screen pressure" for simplicity) is controlled via steel tubes which penetrate the sleeve and represent the in-situ pore pressure in a field situation. The center hole in the sample is fluid filled and the pressure (p_a) is controlled through the end-pistons. The center hole and the pressure p_a represent the borehole and the annulus pressure, respectively, in a field situation. A mineral oil (kerosene) is used as annulus fluid in order to eliminate possible chemical interactions between the annulus fluid and the shale.

The main purpose of these tests is to investigate the sealing capacity of the interface between the casing and the center hole wall, as the pressure difference (σ_{ext} - p_a) causes a reduction of the hole diameter and may bring the hole wall in contact with the casing, potentially generating a shale barrier. To obtain a quantitative measure of the sealing capacity of the shale barrier, the *annulus permeability* is measured during the test. This permeability is the main parameter recorded during these tests. It represents the equivalent permeability of an annulus filling material, giving the same resistance to flow along the annulus as the shale barrier. The annulus permeability is measured periodically during the test, using a transient pressure – pulse decay method, which is less disturbing to the shale barrier than a steady state measurement, and requires less time (Fjær et al., 2018).

The failure characteristics of the center hole will vary with different shale types and the orientation of the center hole with respect to the bedding plane normal. Most often the initial contact between the casing and the yielded sample will not be uniform, and the annulus permeability does not become meaningful until a large portion of the casing length is contacted by the yielded material from the center hole wall. Having three independent measurements of the contact force on the casing gives insight to the pressure distribution which may vary from uniform compression to bending of the casing, however it does not give the full resolution of the variability in the contact pressure. Nevertheless, the initial point of contact between the casing and center hole wall is captured reasonably well.

The annulus pressure p_a is kept equal to p_{sc} throughout the test to maintain uniform pore pressure within the sample. The sample is first allowed to consolidate under conditions where a barrier is unlikely to form; that is, with a low difference between the external stress σ_{ext} and the annulus pressure p_a. After consolidation, the external stress is increased while the screen pressure and the annulus pressure are kept constant. The rate of stress increase is kept low (=0.02 MPa/h) to restrict pore pressure build-up within the sample.

To compare the outcome of the tests, two quantities have been selected as relevant measures of the barrier forming process:

$\sigma'_{cc} = \sigma_{ext} - p_{sc}$ when casing contact is first detected. This is an indicator of the net lateral in situ stress (i.e. the net in situ stress in the plane normal to the borehole axis) required to close the annulus. We call this quantity *annulus closure resistance*.

$\sigma'_{sb} = \sigma_{ext} - p_{sc}$ when the annulus permeability has reached 1 mD. This is an indicator of the net lateral in situ stress required to obtain a specific sealing efficiency. We call this quantity *shale barrier resistance*.

Note that a low value for σ'_{sb} indicates a high degree of willingness to form a shale barrier, and vice versa.

Some of the materials were tested with a different procedure, where the external stress is kept constant while the annulus pressure is reduced stepwise (Fjær et al., 2018). As repeated tests with the "standardized" procedure described above were not possible for all materials, we wish to also utilize the results from such non-standard (underbalanced) tests to get some idea of the performance of these materials. To do so, we try to find the estimated net external stress $\sigma'_{est,e}$ where a given event – observed in an underbalanced test – would occur if the test had been standardized. We establish such an estimate by considering the linear elastic solutions for a hollow cylinder, and the conditions for failure at the borehole wall according to the Mohr-Coulomb criterion (see for instance Fjær et al., 2021):

For $p_a = p_{sc}$ (standard conditions) failure occurs at

$$\sigma'_{ext}(=\sigma_{ext} - p_{sc}) = \frac{1}{2}C_0 \tag{1.3}$$

For $p_a < p_{sc}$ (underbalanced conditions) failure occurs at

$$\sigma'_{ext,u} = \frac{1}{2}C_0 - \chi(p_{sc} - p_a) \tag{1.4}$$

where

$$\chi \approx 1 - \frac{1-2\nu_{fr}}{4(1-\nu_{fr})}\alpha\left[1+\frac{\ln\frac{R_o}{R}-1}{\ln\frac{R_o}{R}}\right] \quad (1.5)$$

C_0 is the unconfined compressive strength, R and R_0 are the inner and outer radii of the hollow cylinder, α is the Biot coefficient, and ν_{fr} is Poisson's ratio. With typical values for these parameters, we find that $\chi \approx 0.75 \pm 0.1$.

By combining expressions (1.3) and (1.4), we find that if failure occurs at $\sigma'_{ext,u}$ in an underbalanced test it should occur at

$$\sigma'_{ext,e} = \sigma'_{ext,u} + \chi(p_{sc} - p_a) \quad (1.6)$$

in a standardized test. Thus, $\sigma'_{ext,e}$ as expressed by Eq. (1.6) may be used as an estimate of the relevant net effective stress for the non-standardized shale barrier tests. Note that underbalance was achieved by stepwise quick reductions of annulus pressure in the underbalanced tests, which implies that onset of rock-casing contact and 1 mD annulus permeability may have occurred within a range of $\sigma'_{ext,e}$ values where observations were absent or hard to interpret, adding further uncertainty to the results. Nevertheless, the materials included here are extreme cases whose results are significant and meaningful even with large uncertainties. In the following, the results originating from the underbalanced tests will be clearly marked.

4. Samples

This study included 9 shales: 6 field cores, labelled F1 ⋯F6, and 3 outcrops, labelled O1, O2, O3. The field cores originate from the North Sea area. The outcrops are known from the literature:

O1 = Pierre II shale (Schultz et al., 1980; Agofack et al., 2022).

O2 = Ølst shale (Heilmann-Clausen et al., 1984; Nielsen et al., 2015).

O3 = Pierre I shale (Schultz et al., 1980; Islam and Skalle, 2013).

Data from petrophysical and rock mechanical characterization of the materials are listed in Table 1.

The rock mechanical parameters are obtained by consolidated undrained (CIU) tests on core plugs oriented with their axis normal to the bedding plane. These parameters are shear modulus G, Poisson's ratio ν, unconfined compressive strength C_0 (UCS), and friction angle Φ which is obtained by combination of results from several tests. Ultrasonic P-wave velocity (V_p) is measured axially during the CIU test, at the end of the consolidation period. S-wave velocity (V_s) is estimated from the initial static unloading shear modulus (obtained by a procedure described by Fjær et al., 2013; see also Lozovyi et al., 2017), and density, presumably representing the velocity at seismic frequencies.

Hollow cylinder strength (HCS) is obtained by a test on a hollow cylinder (outer diameter: 50 mm; inner diameter: 10 mm) and is here defined as the net external stress needed to induce a 1% (10 millistrain) reduction of the hole diameter.

Some of the petrophysical parameters are missing for one of the materials (F6) while most of the rock mechanical parameters are missing for one of the other materials (F5) due to insufficient amounts of available material and other circumstances beyond our control. The test results for these materials are still interesting though. For material F5 we have tentatively filled in most of the missing information based on well-established correlations with available parameters. Results originating from data obtained by this procedure will be clearly marked in the following.

In anisotropic rocks like shale, the direction of the wellbore relative to the bedding plane may have a strong impact on borehole stability (Økland and Cook, 1998). For the field cores in our study, the sample axis has to coincide with the core axis, hence the angle between the borehole and the bedding plane of the shale is fixed by azimuth and inclination of the well relative to strike and dip-angle of the shale bedding. Most of these cores were taken from vertical well sections in shales with horizontal bedding, hence the borehole is nearly normal to the bedding plane for these cores. The same orientation was chosen for the outcrop samples. Effects of wellbore inclination versus bedding plane are therefore not included in this study. Sample F5 is an exception; the angle between borehole and bedding plane is 55° in this sample, corresponding to 35° well inclination in a formation with horizontal bedding. For a strongly anisotropic rock, this inclination may be sufficient to reduce the borehole strength somewhat (Bautmans et al., 2018), hence it is possible that the observed value for σ'_{cc} is lower than it would have been if the borehole was normal to the bedding. The effect is probably limited though. The possible effect on σ'_{sb} is less clear. F5 is marked and may easily be identified in the results presented below.

4. Results

The timeline for the shale barrier test on material O1 is shown in Fig. 2, as an example. Following the initial loading, the sample is left to consolidate for about 12 days at a net external stress of 2 MPa. After that, the external stress is slowly increased. Casing contact is identified as the

Table 1
Petrophysical and rock mechanical data for the tested shales.

Parameter	F1	F2	F3	F4	F5	F6	O1	O2	O3
Density [g/cm^3]	2.14	2.02	2.29	2.30	1.89	2.36	2.06	1.92	2.39
Porosity [%]	39.5	39.7	26.8	21.3	31.9	23.9	40.3	47.5	20.8
Total clay [%]	61.5	85.3	79	62	86.5	47.7	50.5	74.6	45.6
Smectite [%]	48	67	45	49	77	–	86	45	20
Quartz [%]	15	5	9	23	6	26	27	10	27
Spec. surface [m^2/g]	40	17	38.3	8.2	33.2	–	27	54	17
CEC [meq/100g]	53	63.7	64.2	37.1	48.3	42.2	42.6	74.3	26.6
TOC [%]	0.82	3.27	0.65	1.4	3.8	–	1.2	1.2	1.08
V_p [m/s]	2081	2010	2503	2587	1930	2648	2121	1700	2848
V_s [m/s]	611[a]	686[a]	877[a]	829[a]	696[b]	698[a]	535[a]	247[a]	709[a]
Shear modulus [GPa]	0.41	0.33	1.3	1.04	0.26[c]	0.69	0.24	0.0022	0.43
Poisson's ratio [-]	0.43	0.52	0.48	0.43	0.43[d]	0.34	0.38	0.68	0.24
UCS [MPa]	6.3	6.5	12.7	11.5	6.42[e]	9.2	6.4	0.12	9.7
Friction angle [°]	15.1	14.3	19.6	15.2	23.3[f]	25.2	13.3	12.7	30.1
HCS [MPa]	6.4	8.9	10.9	9.7	8.7	7.5	6.5	0.6	11.9

[a] Estimated from initial static unloading modulus (Fjær et al., 2013), and density.
[b] Estimated from P-wave velocity (Castagna et al., 1993).
[c] Estimated from P-wave velocity (Horsrud, 2001).
[d] Estimated from P- and S-wave velocities (Simmons and Brace, 1965).
[e] Estimated from porosity (Dewhurst et al., 2015).
[f] Estimated from clay content (Chang et al., 2006).

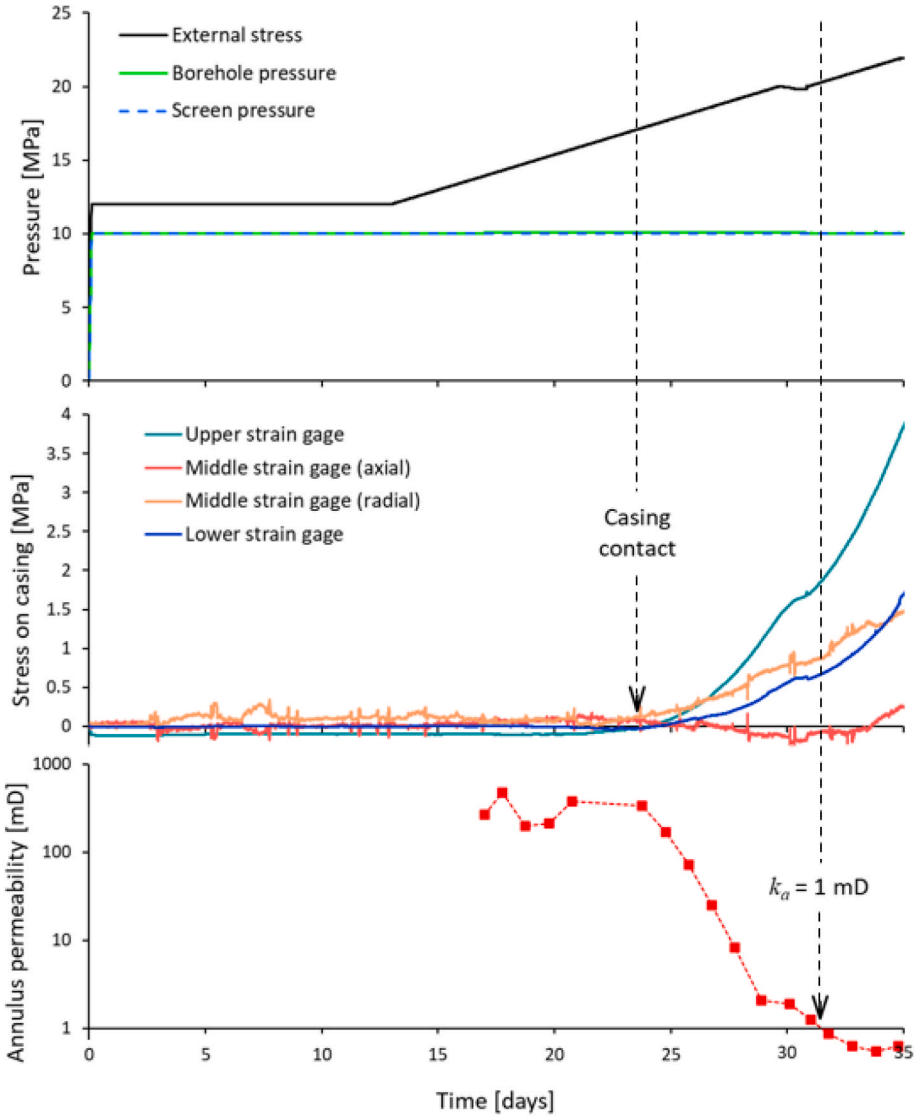

Fig. 2. Timeline for the shale barrier test on O1.

point where a consistent deviation is initiated in at least one of the strain gages attached to the casing. Note that accurate identification of this point is rather challenging and involves an element of subjective judgement, which implies that for most of the tests there is significant uncertainty – typically 1–2 MPa – in the recorded value for σ'_{cc}. The point where the annulus permeability reaches 1 mD is found by interpolation between the recorded values. This is essentially an objective procedure, and the uncertainty is therefore correspondingly less for σ'_{sb}.

CT scans taken before and after the test on O1 are shown in Fig. 3. The scans taken after the test show nearly complete closure of the annulus, in agreement with the induced reduction in annulus permeability. The scans also prove that the rock near the borehole has suffered permanent plastic deformation during the test. Some clearly visible axial cracks, which may have developed during unloading of the sample, indicate the extension of the plastified region (Fjær et al., 2018).

The results from all shale barrier tests are given in Table 2. No value for σ'_{cc} could be obtained for sample F6, as this test was performed on a smaller sample with no strain gages attached to the casing. For the samples F4 and O3, the annulus permeability did not reach as low as 1 mD during the tests, hence no values for σ'_{sb} were detected. The highest value for the net external stress explored in each of these two tests is therefore given as a lower limit in Table 2.

The values for annulus closure resistance and shale barrier resistance given in Table 2 can be correlated with the petrophysical and rock mechanical parameters (Table 1), in order to reveal characteristic features of the rocks most likely to form shale barriers.

First, we consider the correlation between annulus closure resistance and hollow cylinder strength (HCS), as we may expect a close relation between these two parameters. The correlation plot is shown in Fig. 4 (left). The correlation is very strong, with correlation coefficient $r = 0.90$. The correlation between shale barrier resistance and HCS (Fig. 4, right) is weaker but still moderately strong, with $r = 0.77$. This makes sense, as annulus closure is a necessary but not sufficient requirement for a sealing barrier, hence the connection between shale barrier resistance and HCS is expected to be weaker than the connection between annulus closure resistance and HCS.

The red, dashed lines shown in Fig. 4 are trend lines, obtained by fitting the data sets to straight lines. These are included as guides for the eye. The arrows on the figure to the right indicate the unexplored ranges for shale barrier resistance for samples F4 and O3, respectively, which did not reach the 1 mD target. The fact that the arrows are crossing the trend line indicates that also these two samples might have supported the same trend, had the tests been extended.

Values for the correlation coefficient r are given in Table 3, for all correlation sets.

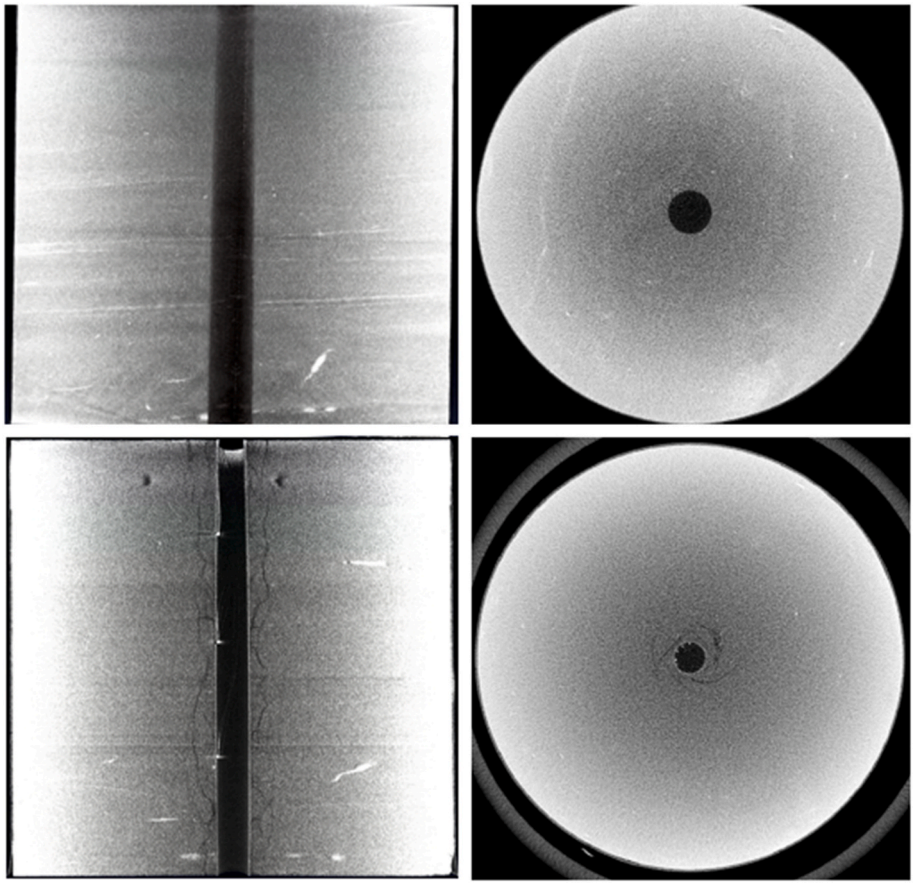

Fig. 3. CT scans of the O1 sample, before the test (upper row; without casing) and after the test (lower row; with casing in place).

Table 2
Test results from the shale barrier tests.

Parameter	F1	F2	F3	F4	F5	F6	O1	O2	O3
σ'_{cc} [MPa]	6	9	9.5	14.4	8.5[c]	–	7.2	1[a]	14.6[a]
σ'_{sb} [MPa]	14.4	10.5	20	>15.2[b]	12.7[c]	21.5[a]	10.6	1.6[a]	>16.6[b]

[a] Underbalanced test – the value is estimated by means of Eq. (1.6).
[b] The target value (k_a = 1mD) was not reached during the test. The given value represents a lower limit for σ'_{sb}.
[c] The angle between the borehole axis and the bedding plane normal is 35° for this sample.

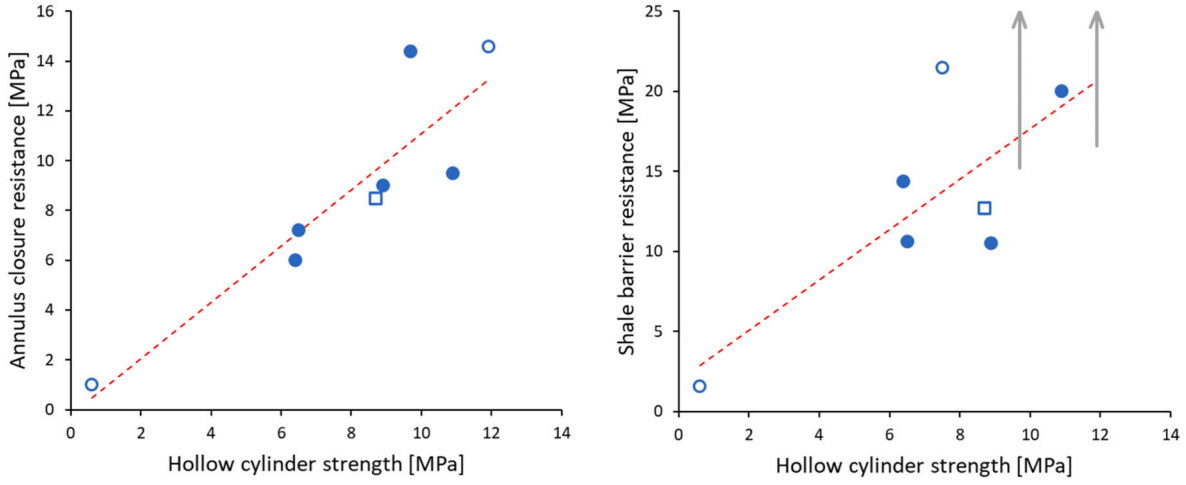

Fig. 4. Correlation plots between hollow cylinder strength (HCS) and annulus closure resistance (left) and shale barrier resistance (right). Open circular symbols (o) represent results from underbalanced tests. The open square symbol (□) represents sample F5 (c.f. footnote c of Table 2). The red dashed lines are linear trend lines.

Table 3
Correlation coefficient r relating annulus closure resistance (σ'_{cc}) and shale barrier resistance (σ'_{sb}) to a petrophysical or rock mechanical parameter.

Petrophysical or rock mechanical parameter	Correlation coefficient r -	
	- with annulus closure resistance	- with shale barrier resistance
Density [g/cm^3]	0.76	0.85
Porosity [%]	−0.93	−0.93
Total clay [%]	−0.34	−0.29
Smectite [%]	−0.31	−0.05
Quartz [%]	0.46	0.30
Spec. surface [m^2/g]	−0.87	−0.32
CEC [meq/100g]	−0.78	−0.55
TOC [%]	0.02	−0.13
V_p [m/s]	0.89	0.93
V_s [m/s]	0.82	0.88
Shear modulus [GPa]	0.58	0.84
Poisson's ratio [-]	−0.76	−0.77
UCS [MPa]	0.84	0.92
Friction angle [°]	0.64	0.85
HCS [MPa]	0.90	0.77

The parameters that appear to have the strongest correlations with shale barrier resistance are porosity, P- and S-wave velocities and UCS ($|r| = 0.88–0.93$). Correlation plots for these parameters are shown in Fig. 5, Fig. 6, Figs. 7 and 8, respectively. Note that the correlation is negative for porosity and positive for P- and S-wave velocities and UCS, meaning that higher porosity indicates higher probability for shale barrier formation while higher P-wave velocity, higher S-wave velocity and higher UCS indicate higher resistance against formation of a shale barrier. Each of these parameters also have strong correlations with annulus closure resistance ($|r| = 0.82–0.93$).

Density, friction angle and shear modulus also have strong correlations with shale barrier resistance ($r \approx 0.85$). The correlations with annulus closure resistance are more moderate ($r = 0.58–0.76$).

All of the mineralogy related parameters correlate poorly with shale barrier resistance. Also the correlation with annulus closure resistance is poor, except for CEC (Fig. 9) and for specific surface (Fig. 10). These somewhat surprising results will be discussed in the next chapter.

5. Interpretation and discussion

Table 3 and Figs. 4–10 show some clear, some less clear and some noticeably absent trends in our data set. This may reveal useful information about characteristic features of the rocks that are most likely to form shale barriers. Note however, there is - statistically - a finite probability that even totally unrelated parameters may display a strong correlation in a given data set. Considering the large number of parameter pairs tested here, and the limited number of samples involved, we may in fact expect to find one or two cases where the parameters correlate strongly simply by chance. Therefore, we shall evaluate the correlations presented in Table 3 carefully and try to back up the findings with theoretical considerations and combination of results.

The very strong correlations ($|r| > 0.85$) between shale barrier resistance and the petrophysical parameters porosity, density, and P- & S-wave velocities agree with earlier findings, as listed in Chapter 1. Although none of these parameters are direct measures of the main parameters mentioned in Chapter 2 – the static shear stiffness and the strength of the rock – they may serve as useful indicators of the rock's ability to form shale barriers since they are often available from well logs.

It seems clear that porosity is a key parameter here. As the presence of solid material is the origin of shear stiffness and shear strength, which provide the resistance against annulus closure and barrier formation, the absence of solid material – i.e. porosity – will have a correspondingly strong impact on the same parameters, as shown by for instance Horsrud (2001). Porosity also has a strong impact on density and wave velocities within the same lithology (Wyllie et al., 1958; Wang, 2000). The correlation between porosity and other parameters from Table 1 are shown in Table 4. Comparing these values to those of Table 3 we see quite clearly that the parameters which have the closest correlation with porosity also have the best correlation to shale barrier resistance. Thus, the strong correlation between for instance P-wave velocity and shale barrier resistance is most likely a consequence of the correlation between P-wave velocity and porosity in our data set, rather than a genuine relationship between P-wave velocity and shale barrier resistance.

Porosity may also be an indicator of another relevant property of the rock. Low porosity is usually a consequence of deep burial and diagenesis at some point in the geological history of the rock, even if the present-day depth is relatively shallow. Over-consolidated materials (i.e., materials that have experienced a higher stress than its present stress level) tend to be more brittle and hence less likely to form a sealing barrier (Holt et al., 2019, 2020), hence porosity may also be an indicator for this relevant property. Over-consolidation can be revealed by p'-q plots of undrained compression tests, as the stress path in such plots make a clear turn to the right at higher stress levels for over-consolidated materials but not for normally consolidated materials. Fig. 11 shows p'-q plots for all the materials in this study (except F5). The four materials F3, F4, F6 and O3 show clear signs of over-consolidation, unlike the others.

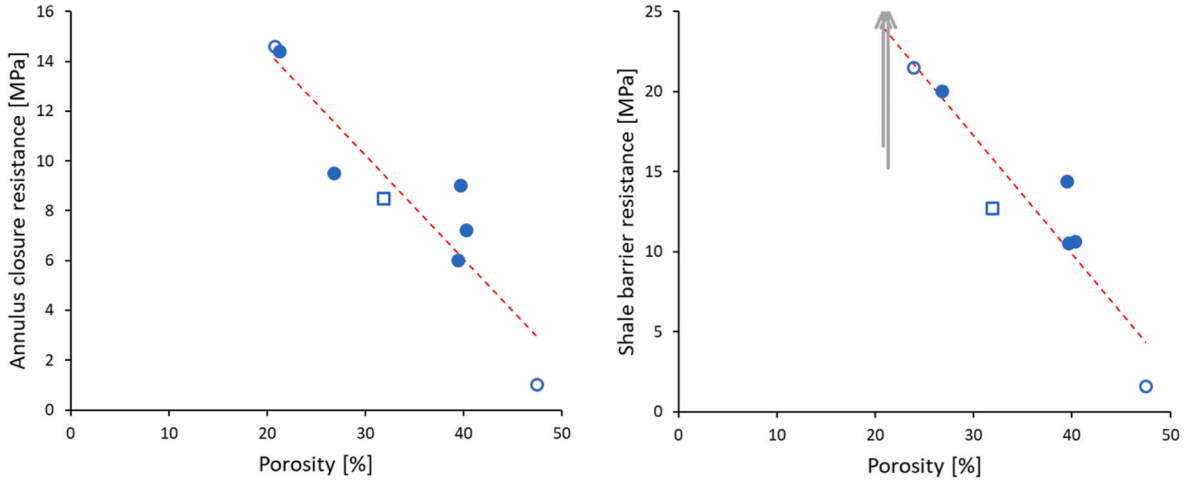

Fig. 5. Correlation plots between porosity and annulus closure resistance (left) and shale barrier resistance (right). Open circular symbols (o) represent results from underbalanced tests. The open square symbol (□) represents sample F5 (c.f. footnote c of Table 2). The red dashed lines are linear trend lines.

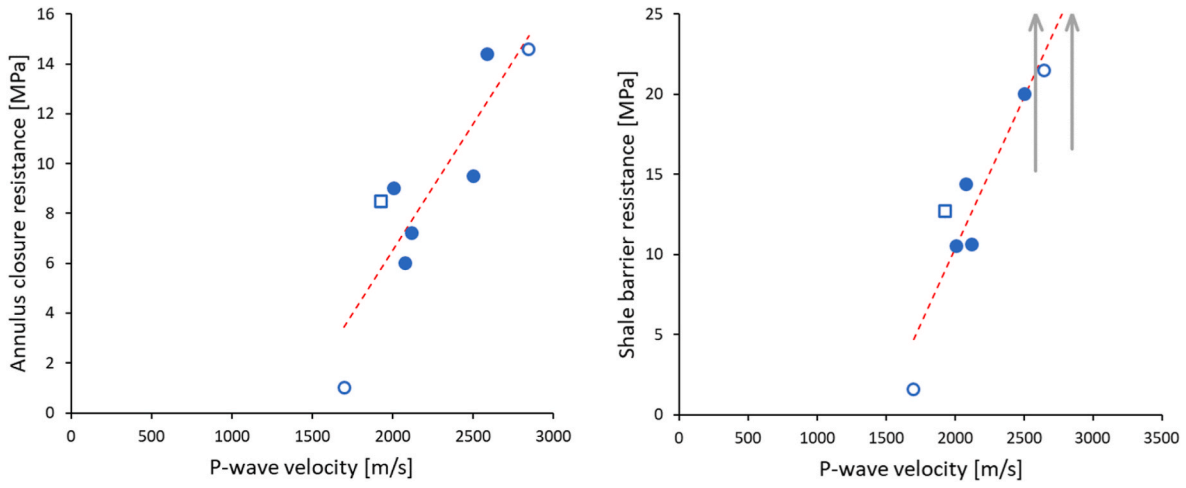

Fig. 6. Correlation plots between P-wave velocity and annulus closure resistance (left) and shale barrier resistance (right). Open circular symbols (o) represent results from underbalanced tests. The open square symbol (□) represents sample F5 (c.f. footnote c of Table 2). The red dashed lines are linear trend lines.

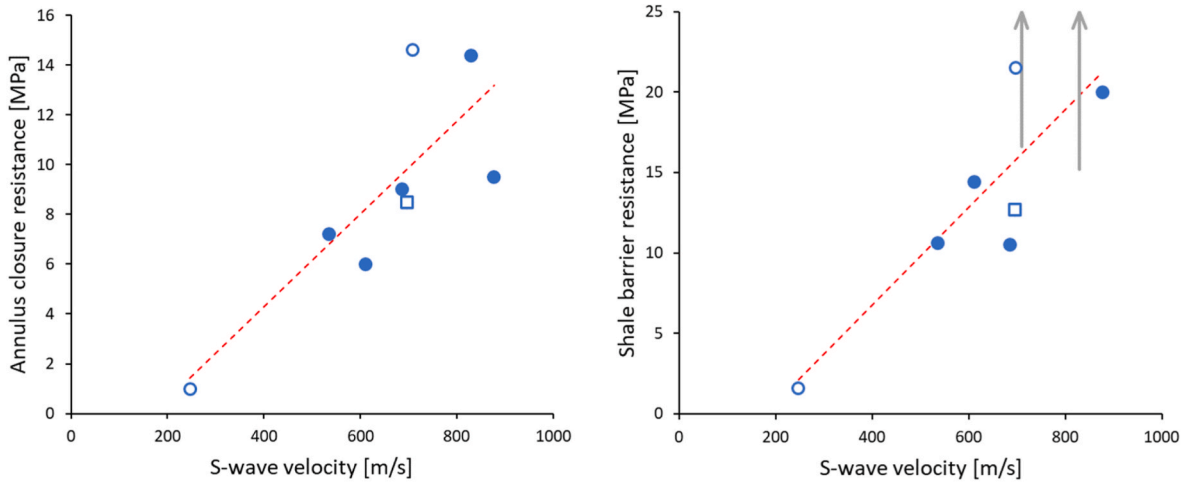

Fig. 7. Correlation plots between S-wave velocity and annulus closure resistance (left) and shale barrier resistance (right). Open circular symbols (o) represent results from underbalanced tests. The open square symbol (□) represents sample F5 (c.f. footnote b of Table 1 and footnote c of Table 2). The red dashed lines are linear trend lines (not including sample F5).

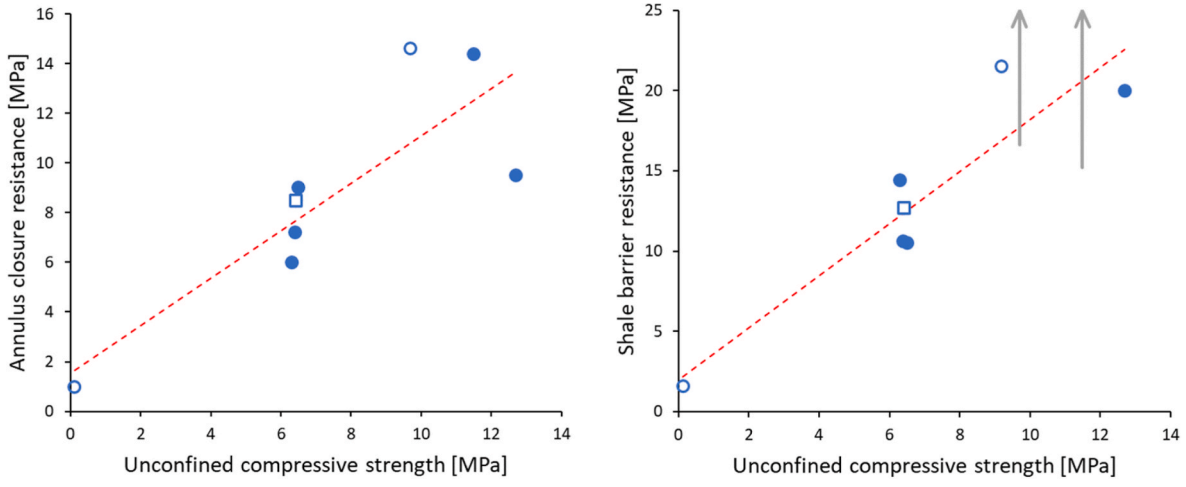

Fig. 8. Correlation plots between unconfined compressive strength (UCS) and annulus closure resistance (left) and shale barrier resistance (right). Open circular symbols (o) represent results from underbalanced tests. The open square symbol (□) represents sample F5 (c.f. footnote e of Table 1 and footnote c of Table 2). The red dashed lines are linear trend lines (not including sample F5).

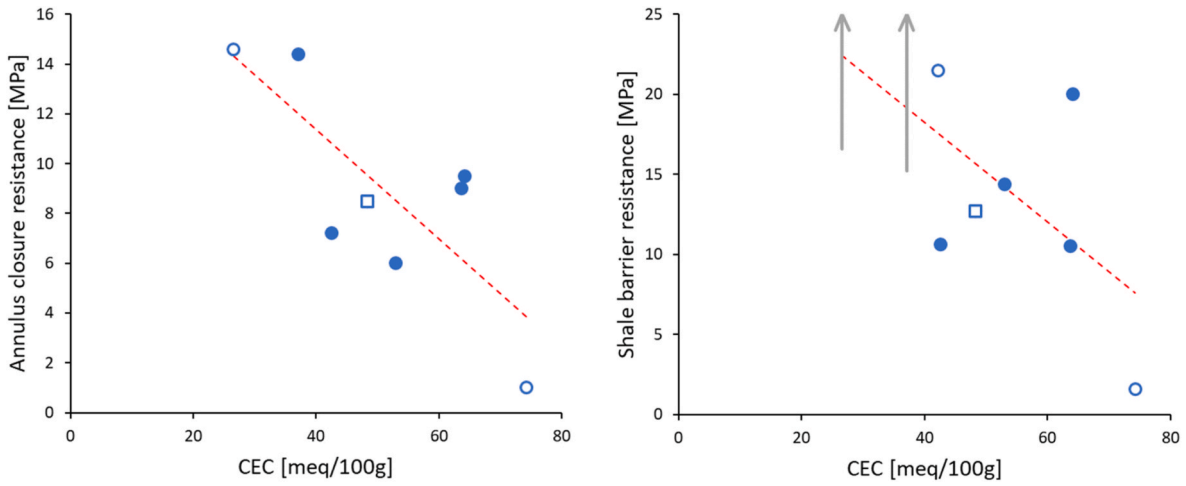

Fig. 9. Correlation plots between CEC and annulus closure resistance (left) and shale barrier resistance (right). Open circular symbols (o) represent results from underbalanced tests. The open square symbol (□) represents sample F5 (c.f. footnote c of Table 2). The red dashed lines are linear trend lines.

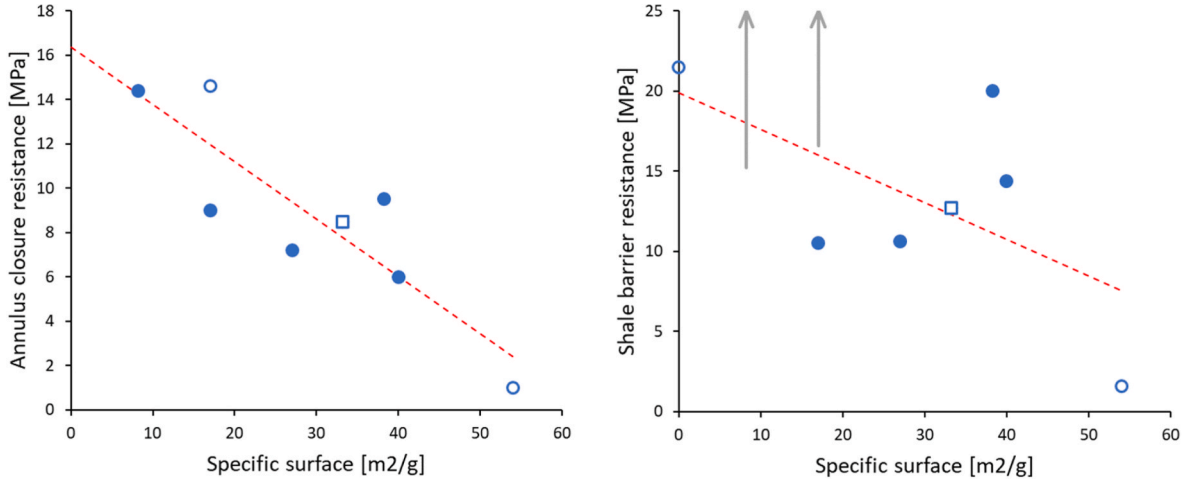

Fig. 10. Correlation plots between specific surface and annulus closure resistance (left) and shale barrier resistance (right). Open circular symbols (o) represent results from underbalanced tests. The open square symbol (□) represents sample F5 (c.f. footnote c of Table 2). The red dashed lines are linear trend lines.

Table 4
Correlation coefficient r for the relations between porosity and the parameters with strongest correlation to porosity.

Parameter	r	Parameter	r
Density	−0.82	UCS	−0.87
P-wave velocity	−0.92	Friction angle	−0.75
S-wave velocity	−0.80	HCS	−0.80
Shear modulus	−0.73	CEC	0.71
Poisson's ratio	0.71	Spec. surface	0.65

These are also the four materials with lowest porosity (Table 1) and highest shale barrier resistance (Table 2).

The correlations between shale barrier resistance and most of the mineralogy related parameters - total clay content, smectite content, quartz content, and total organic carbon (TOC) – do have the expected signs but are all very weak ($|r| < 0.30$). This is surprising, especially as high clay content and low quartz content are assumed to be important features of barrier forming shales (Williams et al., 2009; Kristiansen et al., 2018; van Oort et al., 2022). The selection of rock types in our data set may be a possible explanation for this result. All the shales tested here have clay content above 45% and quartz content below 30%, thus materials with low clay content and high quartz content have not been

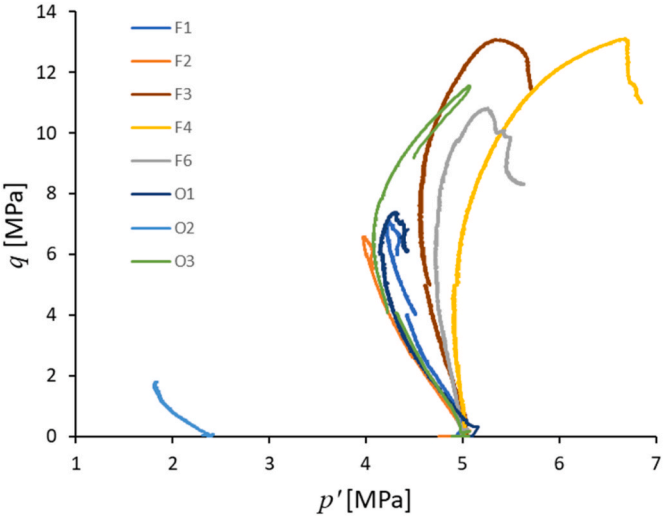

Fig. 11. p'-q plots from a CIU test for all materials, except F5. The O2 sample could not be stabilized at $p' = 5$ MPa, hence this test was run at a lower level. This has no consequence for the conclusion drawn from this plot.

included in the study. The lack of correlation between shale barrier resistance and clay content in our study may indicate that clay content is less important if it is higher than a given threshold. Similarly, quartz content may be less important as long as it is lower than a given threshold.

Such a threshold could be the transition point where stiffer, non-clay components like quartz and carbonates no longer constitute a load-bearing framework. The requirement for the clay content c_{sh} of a shale barrier material may then be expressed as

$$c_{sh}[\%] > \frac{\varphi_{cr} - \varphi}{100 - \varphi} 100 \tag{1.7}$$

where φ is porosity and φ_{cr} is the critical porosity (Nur et al., 1998) for the non-clay components. The value for φ_{cr} varies considerably among rock types (Mavko et al., 2003) but falls in the range 40–65% for the most relevant types. Considering the values given in Table 1, we find that all our materials appear to comply with Eq. (1.7). The least willing ones to form a barrier, O3 and F6, are somewhat marginal though. Although not directly comparable, we also see that the predictions of Eq. (1.7) are on the same page as the individual thresholds for porosity (>25%–30%) and clay content (>50%) given by van Oort et al. (2022). These observations provide some support for the relevance of Eq. (1.7).

Based on the same argument, we may also establish a requirement for the content c_q of quartz and other stiff components:

$$c_q[\%] < \frac{100 - \varphi_{cr}}{100 - \varphi} 100 \tag{1.8}$$

A check on the values given in Table 1 confirms that all our materials fulfil this requirement with a clear margin. Again, we cannot make a direct comparison with the individual threshold ($c_q < 30\%$) given by van Oort et al. (2022), however it is clear that Eq. (1.8) describes a significantly higher threshold. A possible explanation for this discrepancy can be that Eq. (1.8) does not account for matrix cementation.

The cation exchange capacity (CEC) correlates moderately ($r = -0.55$) with shale barrier resistance, and strongly ($r = -0.78$) with annulus closure resistance (Table 3 and Fig. 9). These relations may be realistic, as annulus closure is a necessary but not sufficient requirement for a shale barrier. (Note that the correlation between shale barrier resistance and annulus closure resistance is 0.82.) However, the results do not suggest that CEC is a good indicator for the willingness to form shale barriers.

Even less convincing are the results for the specific surface, which correlates very strongly ($r = -0.87$) with annulus closure resistance, but poorly ($r = -0.32$) with shale barrier resistance (Table 3 and Fig. 10). The possibility that the strong correlation with annulus closure resistance is a statistical coincidence must be considered.

This study has been based on a simplified description of the shale barrier problem, in terms of stress geometry, hole size, duration of test, etc. According to this description, a shale barrier should be formed if the difference between in situ stress σ_h and pore pressure p_{fo} is larger than the shale barrier resistance, i.e. if

$$\sigma_h - p_{fo} > \sigma'_{sb} \tag{1.9}$$

In reality, the in situ stress is usually anisotropic so that the parameter represented by σ_h in Eq. (1.9) should be a function of wellbore inclination and all stress components (primarily the compressive stress in the plane normal to the borehole axis). Further, lack of communication between the annulus fluid and the pore fluid, caused for instance by the use of oil based mud, may result in a situation where the parameter represented by p_{fo} in Eq. (1.9) should be replaced by an annulus pressure that is different from p_{fo}. Also note that σ'_{sb} is here associated with the specific value 1 mD for the annulus permeability. Another target value for the annulus permeability would obviously give another value for σ'_{sb}. Time is also an important parameter, which we have not addressed here, as annulus permeability tends to decline with time (Kristiansen et al., 2018; Xie et al., 2019; Fjær et al., 2016, 2023). For comparisons between standardized tests with identical loading rates, the time issue is essentially eliminated, however. Finally, specific conditions such as borehole temperature, mud composition etc. as mentioned initially, may also have impact on σ'_{sb}. Therefore, we should not expect that application of Eq. (1.9) in combination with trend lines from Figs. 4–10 will give quantitatively accurate predictions of the likelihood for the formation of shale barriers in a field situation. These trends may still be useful as guidelines, however.

6. Conclusions

We have established a quantitative classification of shales in terms of their willingness to form shale barriers. The classification is related to a dedicated laboratory test that is designed to resemble the geometry and stress conditions around a borehole. The classification is based on two parameters:

1. annulus closure resistance, which indicates the net lateral in situ stress required to close the annulus.
2. shale barrier resistance, which indicates the net lateral in situ stress required to obtain a specific sealing efficiency for the barrier.

The definition of the parameters reflects the fact that formation of a shale barrier is a process that depends not only on the rock itself but also on the in situ stress conditions as well as the borehole orientation. It also shows the need to identify a quality requirement for the shale barrier.

Compilation of petrophysical data, rock mechanical data and data from shale barrier tests for a set of field and outcrop shales has revealed some characteristic features of the shales that are most willing to form shale barriers. As expected from theoretical considerations, high shear stiffness and high shear strength coincides with high resistance against annulus closure and shale barrier formation. These parameters are closely related to porosity which emerges as a key parameter in this study: low porosity implies high resistance against annulus closure and shale barrier formation while high porosity indicates a potential willingness to form a shale barrier. Additional features such as over-consolidation may strengthen this relation between porosity and shale barrier resistance. Our results support the assumption that over-consolidated materials are less likely to form sealing barriers.

Other parameters that are closely related to porosity, such as density and P- and S-wave velocities, also correlate well with shale barrier resistance. These parameters are usually available from well logs. Our results may thus enhance the value of well log data as input for shale barrier prediction.

No clear correlation was found between neither total clay content nor quartz content and shale barrier resistance, contrary to expectations. This may be a consequence of the limited selection of materials in our study, which only included shales with clay content above 45% and quartz content lower than 30%. It may also indicate that clay content is less important if it is higher than a given threshold, and similarly that quartz content is less important if it is lower than a given threshold.

CRediT authorship contribution statement

Erling Fjær: Funding acquisition, Conceptualization, Formal analysis, Writing – original draft. **Jørn F. Stenebråten:** Methodology, Data curation, Writing – review & editing. **Sigurd Bakheim:** Investigation, Data curation, Writing – review & editing. **Idar Larsen:** Funding acquisition, Data curation, Writing – review & editing.

Declaration of competing interest

The authors declare that they have no known competing financial interests or personal relationships that could have appeared to influence

the work reported in this paper.

Data availability

The authors do not have permission to share data.

Acknowledgements

This work was supported by the Research Council of Norway, Aker BP ASA, BP Exploration Operating Company Ltd, ConocoPhillips Skandinavia AS, Equinor Energy AS, Lundin Norway AS, Petrobras, Total E&P Norge AS and Vår Energi through the KPN project "Shale Barrier Toolbox: Designing future wells for efficient completion and simpler P&A" (Grant no. 280650/E30) at SINTEF Industry.

References

Agofack, N., Cerasi, P., Sønstebø, E., Stenebråten, J., 2022. Thermo-poromechanical properties of Pierre II shale. Rock Mech. Rock Eng. 55, 6703–6722. https://doi.org/10.1007/s00603-022-02994-6.

Bauer, A., Stenebråten, J.F., Li, L., Fjær, E., 2017. Can Heating-Induced Creep Result in Shale Barriers for P&A Applications? 51st US Rock Mechanics/Geomechanics Symposium. ARMA, pp. 17–818.

Bautmans, P., Fjær, E., Horsrud, P., 2018. The effect of weakness patches on wellbore stability in anisotropic media. Int. J. Rock Mech. Min. Sci. 104, 165–173. https://doi.org/10.1016/j.ijrmms.2018.01.016.

Castagna, J.P., Batzle, M.L., Kan, T.K., 1993. Rock physics – the link between rock properties and AVO response. In: P Castagna, J., Backus, M. (Eds.), Offset-Depende3nt Reflectivity – Theory and Practice of AVO Analysis, Investigations in Geophysics. SEG, pp. 135–171. No 8.

Chang, C., Zoback, M.D., Khaksar, A., 2006. Empirical relations between rock strength and physical properties in sedimentary rocks. J. Pet. Sci. Eng. 51, 223–237. https://doi.org/10.1016/j.petrol.2006.01.003.

Dewhurst, D.N., Sarout, J., Delle Piane, C., Siggins, A.F., Raven, M.D., 2015. Empirical strength prediction for preserved shales. Mar. Petrol. Geol. 67, 512–525. https://doi.org/10.1016/j.marpetgeo.2015.06.004.

Enayatpour, S., Thombare, A., Aldin, M., van Oort, E., 2019. Exploiting shale creep deformation to create annular barriers for well plugging and abandonment: experimental investigation and numerical simulation. SPE-195966-MS. https://doi.org/10.2118/195966-MS.

Fjær, E., Larsen, I., 2018. Shale as a Sealing Barrier Around Deep Wells, 37th International Conference on Ocean. Offshore and Arctic Engineering, pp. OMAE2018–78749. https://doi.org/10.1115/OMAE2018-78749.

Fjær, E., Stroisz, A.M., Holt, R.M., 2013. Elastic dispersion derived from a combination of static and dynamic measurements. Rock Mech. Rock Eng. 46, 611–618. https://doi.org/10.1007/s00603-013-0385-8.

Fjær, E., Folstad, J.S., Li, L., 2016. How creeping shale may form a sealing barrier around a well. 50th US Rock Mechanics/Geomechanics Symposium. ARMA 16–482.

Fjær, E., Horsrud, P., Bautmans, P., 2017. Scaling issues in hollow cylinder tests on shale. In: 51st US Rock Mechanics/Geomechanics Symposium. ARMA, pp. 17–332.

Fjær, E., Stenebråten, J.F., Bakheim, S., 2018. Laboratory test for studies on shale barrier formation, 52nd US Rock Mechanics/Geomechanics Symposium. ARMA 18–1146.

Fjær, E., Holt, R.M., Horsrud, P., Raaen, A.M., Risnes, R., 2021. Petroleum Related Rock Mechanics, third ed. Elsevier, Amsterdam.

Fjær, E., Bakheim, S., Stenebråten, J.F., 2023. Long-term development of shale barrier efficiency: laboratory tests on an outcrop shale. 57th US Rock Mechanics/Geomechanics Symposium. ARMA 23–612.

Gawel, K., Lozovyi, M., Bhuiyan, M.H., Bjørge, R., Fjær, E., 2021. Acid treatment as a way to reduce shale rock mechanical strength and to create a material prone to the formation of permanent well barrier. Energies 14 (2021), 2342. https://doi.org/10.3390/en14092342.

Heilmann-Clausen, C., Nielsen, O.B., Gersner, F., 1984. Lithostratigraphy and depositional environments in the upper paleocene and eocene of Denmark. Bull. Geol. Soc. Den. 33, 287–323. https://doi.org/10.37570/bgsd-1984-33-26.

Holt, R.M., Fjær, E., Larsen, I., Stenebråten, J.F., Raaen, A.M., 2019. On the border between brittle and ductile behavior of shale. In: 53rd US Rock Mechanics/Geomechanics Symposium. ARMA 19-2179.

Holt, R.M., Larsen, I., Fjær, E., Stenebråten, J.F., 2020. Comparing mechanical and ultrasonic behaviour of a brittle and a ductile shale: relevance to prediction of borehole stability and verification of shale barriers. J.Petr.Sci. & Eng. 187, 106746 https://doi.org/10.1016/j.petrol.2019.106746.

Horsrud, P., 2001. Estimating mechanical properties of shale from empirical correlations. SPE Drill. Complet. 16 (2), 68–73. https://doi.org/10.2118/56017-PA.

Islam, M.A., Skalle, P., 2013. An experimental investigation of shale mechanical properties through drained and undrained test mechanisms. Rock Mech. Rock Eng. 46, 1391–1413. https://doi.org/10.1007/s00603-013-0377-8.

Kristiansen, T.G., Dyngeland, T., Kinn, S., Flatebø, R., Aarseth, N.A., 2018. Activating shale to form well barriers: theory and field examples. SPE-191607-MS. https://doi.org/10.2118/191607-MS.

Kristiansen, T.G., Delabroy, L., Palacio, G.A.O., Winther, T., Aarseth, N.A., Bauer, A., Hagenes, K., Lindal, A., Tyberø, P., 2021. Implementing a strategy for shale as well barrier in new wells. SPE/IADC-204075-MS. https://doi.org/10.2118/204075-MS.

Lozovyi, S., Sirevaag, T., Szewczyk, D., Bauer, A., Fjær, E., 2017. Non-elastic effects in static and dynamic rock stiffness. 51st US Rock Mechanics/Geomechanics Symposium, ARMA 17–293.

Mavko, G., Mukerji, T., Dvorkin, J., 2003. The Rock Physics Handbook. Tools for Seismic Analysis in Porous Media. Cambridge University Press.

Nielsen, O.B., Rasmussen, E.S., Thyberg, B.I., 2015. Distribution of clay minerals in the northern North Sea basin during the paleogene and neogene: a result of source-area geology and sorting processes. J. Sediment. Res. 85 (6), 562–581. https://doi.org/10.2110/jsr.2015.40.

Noble, L., Vindheim, H., Govil, A., Obando, G., Haga, J., Shams, A., 2019. Study of Formation Bonding in the Wells of the Varg Field Based on Ultrasonic and Sonic Wireline Log Data. https://doi.org/10.2118/194172-MS. SPE/IADC-194172.MS.

Nur, A., Mavko, G., Dvorkin, J., Galmudy, D., 1998. Critical porosity: the key to relating physical properties to porosity in rocks. Lead. Edge 17, 357–362. https://doi.org/10.1190/1.1437977.

Økland, D., Cook, J.M., 1998. Bedding-related instability in high-angle wells. SPE/ISRM 47285. https://doi.org/10.2118/47285-MS.

Schultz, L.G., Tourtelot, H.A., Gill, J.R., Boerngen, J.G., 1980. Composition and Properties of the Pierre Shale and Equivalent Rocks, Northern Great Plains Region. Geological Survey Professional Paper 1064-B, pp. 1–114. https://doi.org/10.3133/pp1064B.

Simmons, G., Brace, W.F., 1965. Comparison of static and dynamic measurements of compressibility of rocks. J. Geophys. Res. 70, 5649–5656. https://doi.org/10.1029/JZ070i022p05649.

van Oort, E., Juenger, M., Aldin, M., Thombare, A., McDonald, M., Lucas, A., Ditlefsen, F., 2020. Simplifying well abandonment using shale as a barrier. SPE 199654. Revised version: SPE Drill. Complet. 2022 https://doi.org/10.2118/199654-PA.

van Oort, E., Thombare, A., Aldin, M., Lucas, A., 2022. Annular creep barrier evaluation and qualification using ultrasonic measurements. IADC/SPE-208782-MS. https://doi.org/10.2118/208782-PA.

Vrålstad, T., Saasen, A., Fjær, E., Øia, T., Ytrehus, J.D., Khalifeh, M., 2019. Plug & abandonment of offshore wells: ensuring long-term well integrity and cost-efficiency. J. Pet. Sci. Eng. 173, 478–491. https://doi.org/10.1016/j.petrol.2018.10.049.

Wang, Z., 2000. Velocity-density relationships in sedimentary rocks. In: Wang, Z., Nur, A. (Eds.), Seismic and Acoustic Velocities in Reservoir Rocks, Geophysics Reprint Series, No 19. SEG.

Williams, S., Carlsen, T., Constable, K., Guldahl, A., 2009. Identification and qualification of shale annular barriers using wireline logs during plug and abandonment operations. SPE/IADC119321. In: SPE/IADC Drill. Conf. & Exh., Amsterdam, Netherlands https://doi.org/10.2118/119321-MS.

Wyllie, M.R.J., Gregory, A.R., Gardner, G.H.F., 1958. An empirical investigation of factors affecting elastic wave velocities in porous media. Geophysics 23 (3), 459–493.

Xie, X., Fjær, E., Detournay, E., 2019. Time-dependent closure of a borehole in a viscoplastic rock. Geomech. Energy Environ 19, 100115. https://doi.org/10.1016/j.gete.2019.02.001.

Xie, X., Bauer, A., Stenebråten, J.F., Bakheim, S., Lavrov, A., Fjær, E., Kristiansen, T.G., 2020. Can heating induce borehole closure? Rock Mech. Rock Eng. 53, 5715–5744. https://doi.org/10.1007/s00603-020-02238-5.